

**Drug Delivery**

How to cite:

International Edition: doi.org/10.1002/anie.202100873

German Edition: doi.org/10.1002/ange.202100873

# Structural Transformative Antioxidants for Dual-Responsive Anti-Inflammatory Delivery and Photoacoustic Inflammation Imaging

Caiyan Zhao<sup>+</sup>, Jingxiao Chen<sup>+</sup>, Jiamin Ye<sup>+</sup>, Zhi Li, Lichao Su, Junqing Wang, Ye Zhang, Jinghua Chen, Huanghao Yang, Jinjun Shi,<sup>\*</sup> and Jibin Song<sup>\*</sup>

**Abstract:** We have synthesized a PEGylated, phenylboronic acid modified L-DOPA pro-antioxidant (pPAD) that can self-assemble into nanoparticles (pPADN) for the loading of a model glucocorticoid dexamethasone (Dex) through 1,3-diol/phenylboronic acid chemistry and hydrophobic interactions for more effective treatment of inflammation. Upon exposure to ROS, pPADN convert into the active form of L-DOPA, and a cascade of oxidative reactions transform it into antioxidative melanin-like materials. Concomitantly, the structural transformation of pPADN triggers the specific release of Dex, along with the acidic pH of inflammatory tissue. In a rat model of osteoarthritis, Dex-loaded pPADN markedly mitigate synovial inflammation, suppress joint destruction and cartilage matrix degradation, with negligible *in vivo* toxicity. Moreover, *in situ* structural transformation makes pPADN suitable for noninvasive monitoring of therapeutic effects as a photoacoustic imaging contrast agent.

## Introduction

Inflammation plays a pivotal role in response to danger signals from infection and tissue damage.<sup>[1]</sup> The activated immune system triggered by pathogen-associated molecular patterns or damage-associated molecular patterns then recruits monocytes, polarizes macrophages, and secretes inflammatory mediators such as interleukin-1 and cyclooxygenase-2 (COX-2), promoting the clearance of injury tissue

debris and byproducts.<sup>[2]</sup> However, when this process is out of control, these pro-inflammatory factors would lead to hyperinflammation, resulting in chronic diseases such as autoimmune disease, degenerative disease, cancer, and others.<sup>[3]</sup> It is worth noting that inflammatory responses are often associated with overproduction of reactive oxygen species (ROS).<sup>[4]</sup> Higher levels of toxic ROS not only induce oxidative injury, cell apoptosis and necrosis, but also activate inflammatory signaling through NF- $\kappa$ B, amplify pro-inflammatory pathways, and exacerbate immune responses.<sup>[5]</sup> Of note, the secondary species (e.g.,  $\cdot$ OH,  $\cdot$ OCl, and  $\text{OONO}^-$ ) are more chemically reactive and less controllable than primary species (e.g.,  $\text{O}_2^{\cdot-}$  and  $\text{H}_2\text{O}_2$ ), due to the lack of specific enzyme control systems in the body.<sup>[6]</sup> The persistent presence of these uncontrolled ROS inevitably potentiates inflammation in the lesions. In addition, the infiltration and activation of inflammatory cells induce accelerated glycolysis and increased lactic acid secretion, acidifying the environment of inflamed tissues.<sup>[7]</sup>

Glucocorticoids such as dexamethasone (Dex) play an important role in the treatment of inflammation, as they can quickly slow the progress of inflammation and relieve pain.<sup>[8]</sup> However, glucocorticoids injected into inflamed tissues such as the joint in osteoarthritis (OA) are cleared rapidly.<sup>[9]</sup> In addition, there is always the risk of untoward side-effects through nonspecific targeting, such as suppression of immune function and the risk of inducing diabetes, muscular atrophy, osteoporosis, and other conditions.<sup>[10]</sup> Thus, the use of glucocorticoids is often limited. To achieve better therapeutic efficacy and minimize adverse effects, new approaches that can prolong the retention time of glucocorticoids at the site of inflammation and control drug release locally in lesions with minimal exposure of normal tissues are sought.

Herein, we report a transformative antioxidative biomaterial-based platform for ROS and pH dual-responsive Dex delivery to effectively treat OA. Biomaterials with intrinsic ROS scavenging activity have recently gained significant attention, among which nano-antioxidants composed of natural biomolecules represent a promising paradigm for treatment of ROS-related diseases.<sup>[4c,11]</sup> Particularly, dopamine or L-DOPA with catechol structure has been widely suggested as an effective antioxidant; it can be readily oxidized to form cross-linked polydopamine (a major pigment of melanin) in an oxidative environment.<sup>[12]</sup> Melanin, a natural antioxidative metabolite, has also been applied in antioxidative treatment.<sup>[13]</sup> However, these melanin-based/like biomaterials are associated with several drawbacks, such as limited stability due to autooxidation of catechol in aqueous solution

[\*] Dr. C. Zhao,<sup>[†]</sup> J. Ye,<sup>[†]</sup> Dr. Z. Li, L. Su, Prof. H. Yang, Prof. J. Song MOE Key Laboratory for Analytical Science of Food Safety and Biology, College of Chemistry, Fuzhou University, Fujian Science & Technology Innovation Laboratory for Optoelectronic Information of China

Fuzhou 350108 (P. R. China)

E-mail: jibinsong@fzu.edu.cn

Dr. C. Zhao,<sup>[†]</sup> Dr. J. Chen,<sup>[†]</sup> Dr. J. Wang, Dr. Y. Zhang, Prof. J. Shi Center for Nanomedicine, Brigham and Women's Hospital Harvard Medical School

Boston, Massachusetts 02115 (USA)

E-mail: jshi@bwh.harvard.edu

Dr. J. Chen,<sup>[†]</sup> Prof. J. Chen

Key Laboratory of Carbohydrate Chemistry and Biotechnology Ministry of Education, School of Pharmaceutical Sciences Jiangnan University

Wuxi 214122 (P. R. China)

[†] These authors contributed equally to this work.

Supporting information and the ORCID identification number(s) for the author(s) of this article can be found under:

<https://doi.org/10.1002/anie.202100873>.

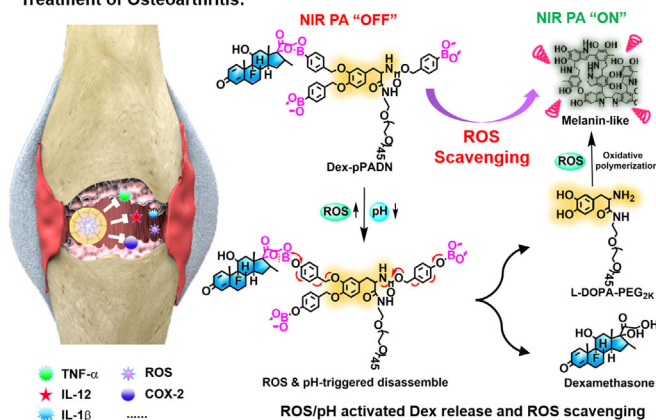
and their complicated structure and variable performance.<sup>[14,15]</sup> Moreover, the use of antioxidative biomaterials for delivery of anti-inflammatory drugs to treat inflammation remains largely unexplored.

In this study, we synthesized a PEGylated, phenylboronic acid modified L-DOPA pro-antioxidant (pPAD) that can self-assemble into nanoparticles (pPADN) for specific loading and dual-responsive delivery of Dex (Scheme 1). Phenylboronic acid is an efficient ROS-responsive group,<sup>[16]</sup> that

#### Preparation of Dex-pPADN:



#### Treatment of Osteoarthritis:



**Scheme 1.** Schematic illustration of the preparation of Dex-pPADN for treatment of osteoarthritis. pPAD is first synthesized via protecting the amine and phenol groups of L-DOPA with phenylboronic acid groups and then PEGylating. Dex-pPADN is formulated by loading Dex with pPAD through 1,3-diol/phenylboronic acid chemistry and hydrophobic interactions. Dex-pPADN dissociates and is transformed into a melanin-like compound in response to excess ROS, along with the release of Dex in acidic inflammatory tissue, which synergistically induces the inhibition of pro-inflammatory factors, the scavenging of ROS, and the activation of a near-infrared (NIR) photoacoustic (PA) signal.

allows the transformation of pPAD to active L-DOPA upon oxidant trigger and through further oxidation to form melanin-like structure. Therefore, the pPAD scaffold is expected to play an antioxidant role in the presence of excess ROS. Moreover, the boronic ester formed from phenylboronic acid and diol is known to be one of the strongest single-pair reversible functional group interactions in aqueous solution. It has been widely used to construct glucose and pH sensors, among which 1,2- or 1,3-diols bind particularly easily with phenylboronic acid due to the formation of stable five- or six-membered ring structures.<sup>[17]</sup> Thus, the 1,3-diol present on glucocorticoids provides an ideal site for interaction with phenylboronic acid, which along with the hydrophobic interaction, leads to specific and high Dex loading and controllable Dex release. In addition, mPEG<sub>2k</sub>-NH<sub>2</sub> becomes linked to the carboxyl group of L-DOPA to form amphiphilic

pPAD, enabling self-assembly into stable pPADN. In a rat model of OA, the therapeutic effect of Dex-loaded pPADN was evaluated. Additionally, based on the photoacoustic (PA) imaging feature of melanin nanomaterials,<sup>[18]</sup> and the widely exploration of PA imaging in measuring oxidative stress,<sup>[19]</sup> the use of pPADN for ROS-specific PA imaging performance was explored.

## Results and Discussion

To endow the unstable antioxidant L-DOPA with controllable, intelligent and stable performance, its phenol and amine groups were sequentially protected by self-immolative and ROS-responsive phenylboronic acid groups, which can also reversibly bind with the 1,3-diols present in glucocorticoids. To make it amphiphilic, mPEG<sub>2k</sub>-NH<sub>2</sub> was then coupled to the carboxyl group of L-DOPA to form PEGylated phenylboronic acid-conjugated L-DOPA (pPAD) polymer (Scheme S1, Figure S1–S11).

The pPAD polymer with hydrophobic block of phenylboronic acid-conjugated L-DOPA derivative and hydrophilic block of PEG was self-assembled into nanoparticles (pPADN) in aqueous solution. In theory, pPADN provided a stable reservoir for Dex on account of the specific and reversible covalent bonding of phenylboronic acid and 1,3-diol, as well as the hydrophobic interaction. To explore the self-assembly process of Dex-pPADN, the interaction of Dex and pPAD was analyzed by isothermal titration calorimetry (ITC). Figure S12 shows the enthalpy change  $\Delta H = -1386 \text{ cal mol}^{-1}$  and the entropy change  $\Delta S = 25.5 \text{ cal mol}^{-1} \text{ deg}^{-1}$ . The titrations were exothermic ( $\Delta H < 0$ ) and spontaneous ( $\Delta G < 0$ ;  $\Delta G = \Delta H - T\Delta S$ ). This suggests that Dex can self-assemble with pPAD to form Dex-pPADN, in which both the phenylboronic acid/1,3-diol chemistry and hydrophobic interaction may play a role. Given the importance of encapsulation efficiency and particle size in nanoparticle drug delivery, these two parameters were then evaluated. As shown in Figure 1 a,b, keeping the concentration of Dex constant at  $1 \text{ mg mL}^{-1}$ , the drug encapsulation efficiency gradually increased while the particle size first decreased and then increased as the ratio of copolymer/drug increased. Dex-pPADN showed an ultrahigh encapsulation efficiency of  $\approx 92\%$  and lowest particle size at the 10:1 mass ratio of pPADN to Dex, which was selected for subsequent investigation. As a ROS non-sensitive control, the PEGylated, phenyl-protected L-DOPA (pBD) was constructed by replacing the phenylboronic acid groups of pPAD with phenyl structures (Scheme S2, Figure S13–S17). Drug encapsulation efficiency and particle size of Dex-pBDN were also analyzed. As shown in Figure S18, the Dex encapsulation efficiency of pBD was significantly lower than that of pPAD at the same polymer/Dex ratios. In addition, the particle size of Dex-pBDN did not decrease as the ratio of polymer/Dex increased (Figure S19). These results may have been caused by the fact that Dex molecules can be specifically bound to pPAD through 1,3-diol/phenylboronic acid chemistry and hydrophobic interaction, but pBD can load Dex only through hydrophobic interaction. The unique interactions between



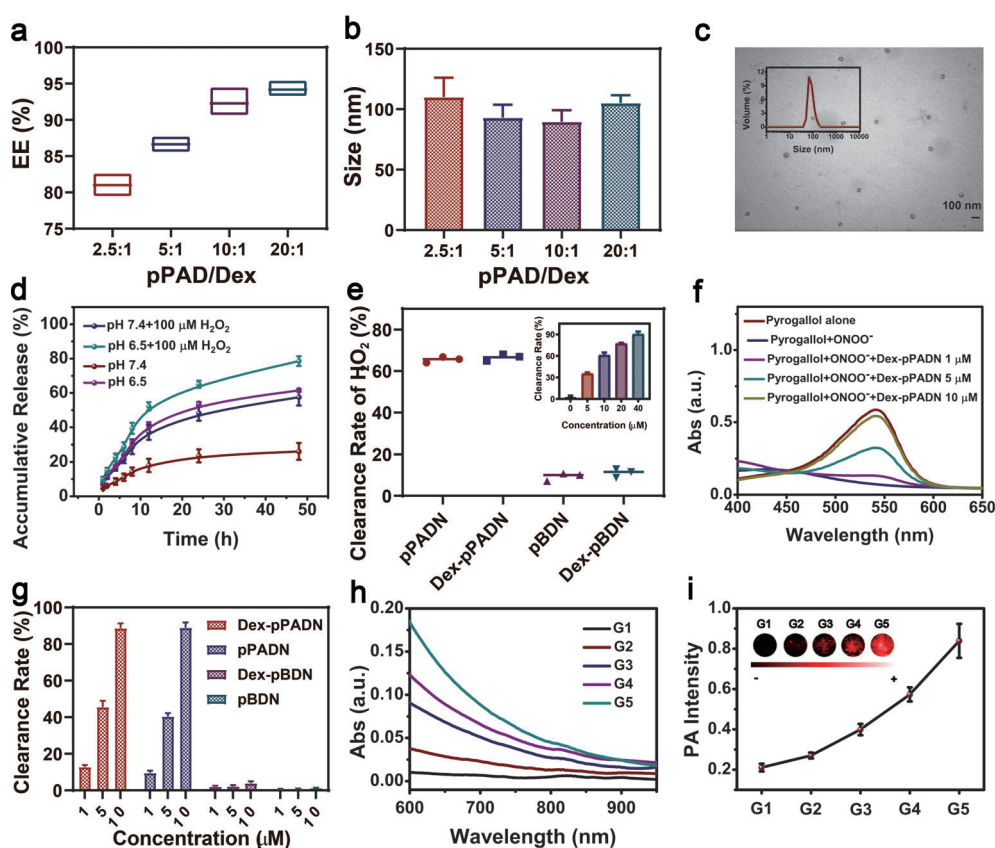


**Figure 1.** Preparation and characterization of Dex-pPADN and related materials. The effects of pPADN/Dex ratios on a) encapsulation efficiency and b) particle size. c) TEM images and hydrodynamic diameter distribution of Dex-pPADN at the pPADN/Dex ratio of 10:1. d) ROS- and pH-triggered release of Dex from Dex-pPADN in vitro. e)  $\text{H}_2\text{O}_2$  scavenging effect of various nanoformulations at the same conditions (concentration of pPADN: 20  $\mu\text{M}$ ; incubation time: 4 h); inset plot shows the  $\text{H}_2\text{O}_2$  scavenging effect of Dex-pPADN with different concentrations (incubation time: 4 h). f)  $\text{ONOO}^-$  scavenging effect of Dex-pPADN with different concentrations (incubation time: 4 h). g) The quantification of the  $\text{ONOO}^-$  scavenging effect of various nanoformulations. h) UV-vis-NIR absorption spectra; i) PA signal intensity and PA images of Dex-pPADN after incubation with different concentrations of  $\text{ONOO}^-$ . (G1: 0 mM  $\text{ONOO}^-$ , G2: 5 mM  $\text{ONOO}^-$ , G3: 10 mM  $\text{ONOO}^-$ , G4: 20 mM  $\text{ONOO}^-$ , G5: 40 mM  $\text{ONOO}^-$ ).

pPADN and Dex improved encapsulation capacity of pPADN for Dex and a certain amount of Dex could condense pPADN into smaller nanostructures.

The physicochemical characteristics of Dex-pPADN were further investigated at the polymer/drug ratio of 10/1. As shown in Figure 1c, dynamic light scattering (DLS) measurements revealed that the hydrodynamic diameter of Dex-pPADN was  $89.6 \pm 9.5$  nm. Transmission electron microscopy showed that the morphology of Dex-pPADN is a homogeneous spherical structure. Subsequently, we investigated the drug release kinetics of Dex-pPADN under inflammatory or physiological environments simulated in vitro. As shown in Figure 1d, Dex was released from Dex-pPADN much more quickly at pH 6.5 and/or in the buffer with  $\text{H}_2\text{O}_2$ , whereas Dex release was slower in the buffer without  $\text{H}_2\text{O}_2$  at pH 7.4. Nearly 79% of encapsulated Dex was released after 48 h under the oxidative and acid condition. In contrast, only approximately 26% of Dex was released after 48 h under conditions similar to the normal physiological environment. These findings suggest the selective release of Dex from Dex-

pPADN, which would definitely be beneficial for improving drug availability and minimizing undesired side effects.

The boronic acid/esters in Dex-pPADN are readily detached after attack by  $\text{ONOO}^-$  and  $\text{H}_2\text{O}_2$ , producing the antioxidative form of L-DOPA. We went on to assess the anti-oxidative performance of Dex-pPADN by studying its  $\text{ONOO}^-$  and  $\text{H}_2\text{O}_2$  scavenging activity. As shown in Figure 1e, Dex-pPADN significantly scavenged  $\text{H}_2\text{O}_2$  in a concentration-dependent manner, but Dex-pBPN and pBPN failed to scavenge  $\text{H}_2\text{O}_2$ . In addition, consistent with the results of the  $\text{H}_2\text{O}_2$ -scavenging assay, Dex-pPADN displayed preferable concentration-dependent  $\text{ONOO}^-$  scavenging ability (Figure 1f,g). Almost 89% of  $\text{ONOO}^-$  was quenched when it was co-incubated with 10  $\mu\text{M}$  of Dex-pPADN. Whereas neither pBPN nor pDex-BPN scavenged  $\text{ONOO}^-$  (Figure S20). These findings imply that the protection of the amine and phenolic groups of L-DOPA is an

effective way to render it stable and inactive. Meanwhile, protection using ROS-responsive boronic acid groups not only preserves its naturally antioxidative activity but also endows it with the unique ability to bind with glucocorticoids.

Antioxidative stability and colloidal structure stability were further evaluated. As shown in Figure S21,S22, the scavenging activity of the Dex-pPADN against both  $\text{H}_2\text{O}_2$  and  $\text{ONOO}^-$  showed no obvious change after 6-month storage. In addition, the hydrodynamic diameter of Dex-pPADN in saline solution can be maintained at  $\approx 90$  nm for at least 6 months (Figure S23). Since glucose could form covalent adducts with boronic acids, we then evaluated the stability of Dex-pPADN in saline solution with the presence of glucose (0.90  $\text{mg mL}^{-1}$ , similar to normal blood glucose content). Results showed that nanoparticle size of Dex-pPADN was not significantly changed and the Dex leakage was less than 1% even after incubation for 7 days (Figure S24). Such good antioxidative stability and structural stability are predictive of its successful advancement to in vivo studies.

L-DOPA monomer is instable and readily undergoes self-polymerization to form a melanin-like structure in an

oxidative environment, coupled with a color change from colorless to dark brown. Polydopamine has a broad absorption band in the near infrared (NIR) region and shows good PA effect. By exploiting these features, we further investigated the ROS-induced variation of Dex-pPADN. UV-vis-NIR absorption and PA imaging performance of Dex-pPADN were studied before and after co-incubation with ONOO<sup>-</sup>. ONOO<sup>-</sup> concentrations ranging from 5 to 40 mM were applied to oxidize Dex-pPADN. As shown in Figure 1h, the UV-vis-NIR absorption spectra revealed that Dex-pPADN showed no absorption in the NIR region, but obviously enhanced absorption signals were observed after the ONOO<sup>-</sup> trigger. Meanwhile, the absorption signals showed an increase in ONOO<sup>-</sup> concentration-dependent manner. In addition, digital picture visually confirmed that the color of Dex-pPADN solution gradually changed from colorless to brown as the increase of ONOO<sup>-</sup> concentrations (Figure S25). PA imaging results were agreed with UV-vis-NIR absorption assay (Figure 1i). As the concentration of ONOO<sup>-</sup> increased, PA signal of Dex-pPADN is significantly enhanced. Next, we used another oxidant, ClO<sup>-</sup> to further study the ROS-mediated oxidation of Dex-pPADN (Figure S26). The color change of the solution from colorless to brown was observed as the concentration of ClO<sup>-</sup> increased, consistent with the ONOO<sup>-</sup> assay. Moreover, the chemical structure change of pPAD in oxidation atmosphere was investigated via <sup>1</sup>H NMR (Figure S27). The reaction with ONOO<sup>-</sup> resulted in a significant change of peaks at  $\delta$  8.0–6.5 ppm from benzene ring, which do not correspond to the protons from monomer L-DOPA. Based on these results, we speculated that not only was pPAD transformed into L-DOPA in the presence of ONOO<sup>-</sup>, but also further oxidized, leading to the formation of melanin-like product.

COX-2 plays an essential role in the development and progression of inflammation. Therefore, COX-2 inhibition activity of Dex-pPADN were evaluated by western blot (WB) in activated macrophage Raw 264.7 cells. LPS is a component of cell walls from Gram-negative bacteria and a toll-like receptor (TLR4) agonist that is widely used as an activator of macrophages to create inflammation models.<sup>[20]</sup> After 15 h of incubation with 1.0  $\mu\text{g mL}^{-1}$  of LPS, significant macrophage activation was observed, as evidenced by upregulated expression of COX-2 (Figure S28). In contrast, when the activated Raw 264.7 cells were treated with Dex-pPADN, the expression of COX-2 was significantly reduced, with a concentration-dependent inhibition effect. Furthermore, the inhibition effect of Dex-pPADN, pPADN, and dexamethasone sodium phosphate (Dex-p, a water-soluble form) against activation of macrophages was compared under the same conditions. As shown in Figure 2a, expression of COX-2 was down-regulated by these drugs. pPADN treatment only moderately suppressed the activation of macrophages with 92% expression of COX-2, whereas treatment with Dex-p or Dex-pPADN dramatically lowered this value to 66% or 30%, respectively.

Excess ROS contributed to inflammation and amplified pro-inflammatory pathways. We went on to investigate ROS levels in LPS-activated Raw 264.7 cells using a commercial kit and 2',7'-dichlorofluorescein diacetate (DCFH-DA). As

shown in Figure S29, ROS was overproduced after LPS stimulation, with bright green fluorescence in Raw 264.7 cells. As expected, Dex-pPADN effectively decreased ROS levels in activated Raw 264.7 cells in a dose-dependent manner; the effective concentration of Dex-pPADN against overproduced ROS was 50  $\mu\text{g mL}^{-1}$ . Furthermore, the ROS scavenging effect of Dex-pPADN, pPADN, and Dex-p was compared (Figure 2b). Both pPADN and Dex-pPADN dramatically reduced levels of overproduced ROS relative to the LPS treatment group. However, Dex-p only slightly decreased ROS levels. Quantitative results from flow cytometry were consistent with the above results obtained with a confocal laser scanning microscope (CLSM) (Figure 2c). Dex-pPADN showed the best effect in inhibiting the generation of both cytotoxic ROS and inflammatory COX-2.

It should be noted that the inflammatory mediators released by activated macrophage can induce different levels of activation, apoptosis, and necrosis of chondrocytes and synoviocytes in OA. Hence the ability of Dex-pPADN to inhibit inflammation-induced death of ATCD5 cells was evaluated by CCK-8. Neither pPADN nor Dex-pPADN elicited obvious cytotoxicity even at high pPADN concentrations such as 400  $\mu\text{g mL}^{-1}$  (Figure S30). However, the viability of ATCD5 cells showed dose-dependent decrease after incubation with the cell supernatant harvested from LPS activated macrophages (Figure S31). When the concentration of cell supernatant was 20%, the death rate of ATCD 5 cells reached  $\approx 45\%$ . In comparison, treatment with Dex-pPADN (100  $\mu\text{g mL}^{-1}$  of pPADN) reduced this value to  $\approx 5\%$  (Figure 2d). In addition, annexin V-FITC/PI co-staining assay verified that the supernatant harvested from activated macrophages induced apoptosis in ATCD5 cells, which was significantly reversed by pre-treatment or post-treatment with Dex-pPADN. As shown in Figure 2e–f, the presence of cellular supernatant harvested from LPS-activated macrophages caused apoptosis in 51.73% of ATCD5 cells; pre/post-treatment with Dex-pPADN reduced this value to 18.91 or 27.23%, respectively. Further study using TUNEL assay also revealed that the apoptosis status of ATCD5 cells induced by inflammatory mediators from activated macrophage was effectively reversed via pre/post-treatment with Dex-pPADN (Figure 2g), suggesting that Dex-pPADN protected ATCD5 cells from damage by pro-inflammatory factors.

Given the promising anti-inflammatory activity of Dex-pPADN in vitro, its efficacy in treating OA was evaluated in a rat model. Following arthritis induction, Dex-pPADN were delivered into arthritic knees via intra-articular injection every 4 days (Figure 3a).

Healthy rats injected with PBS and OA rats injected with PBS, pPADN, or Dex-p served as controls. The degree of swelling in knee joints was assessed by measuring knee width. As shown in Figure S32, OA mice developed severe swelling of knee joints. After Dex-pPADN treatment, knee joint swelling was dramatically ameliorated, showing the strongest therapeutic efficacy (Figure 3b). Treatment with either pPADN or Dex-p only moderately suppressed knee joint swelling. At the study endpoint, the knee joints in different treatment groups were photographed and compared. As shown in Figure 3c, arthroncus was clearly observed in the



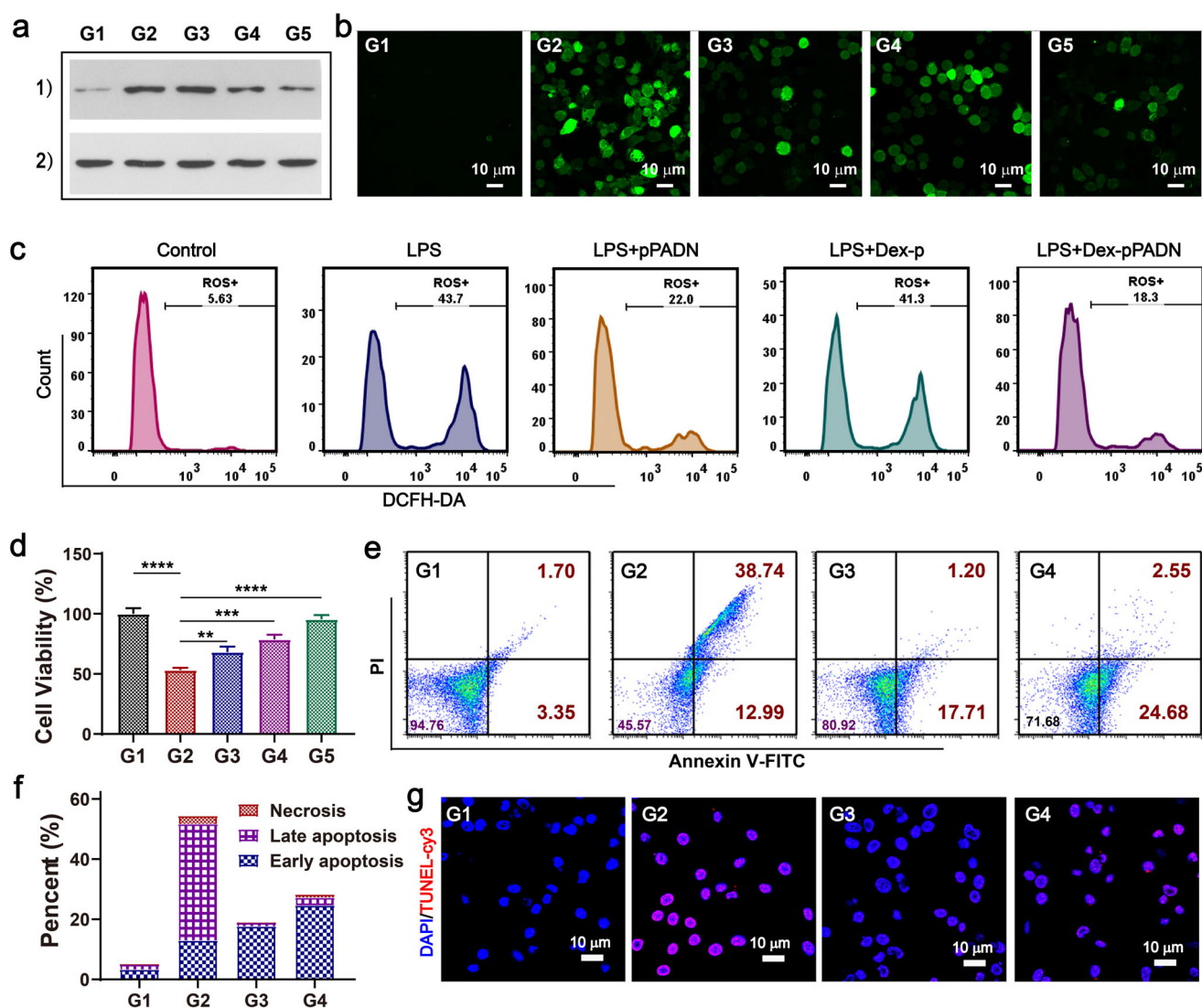


**Figure 2.** Anti-inflammatory, anti-oxidative, and cellular protective activities of Dex-pPADN. a) COX-2 expression in Raw 264.7 cells detected by Western blot. (Lane 1: COX-2; Lane 2: GAPDH). b) ROS levels in Raw 264.7 cells visualized with a confocal laser scanning microscope (CLSM). G1: PBS; G2: LPS; G3: LPS + pPADN; G4: LPS + Dex-p; and G5: LPS + Dex-pPADN. c) ROS levels in Raw 264.7 cells analyzed by flow cytometry. d) Cell viabilities of ATCD5 cells under different treatment conditions (G1: untreated control; G2–G5: treated with supernatant collected from activated Raw264.7. G2: PBS; G3: 25  $\mu\text{g mL}^{-1}$  of Dex-pPADN; G4: 50  $\mu\text{g mL}^{-1}$  of Dex-pPADN; G5: 100  $\mu\text{g mL}^{-1}$  of Dex-pPADN). e) Flow cytometry analysis of ATCD5 cells. f) Quantitative analysis of apoptotic and necrotic ATCD5 cells. g) Merged CLSM images of ATCD5 cells under different treatment conditions. (e–g: G1: untreated control; G2–G4: treated with supernatant collected from activated Raw264.7. G2: PBS; G3: pre-treated with Dex-pPADN; G4: post-treated with Dex-pPADN). Statistical significance was calculated by *t*-test ( $n = 3$ ): \*\*  $p < 0.01$ , \*\*\*  $p < 0.005$ , and \*\*\*\*  $p < 0.001$ .

OA model group, but the symptoms in the Dex-pPADN treatment group were significantly alleviated to a level comparable to that of healthy mice. It has been reported that inflammation in OA is often accompanied by hyperthermia in knee joints due to the increased synovitis and/or subchondral bone activity.<sup>[21]</sup> Thus thermography of knee joints was recorded using a digital infrared thermal imaging camera at the study endpoint to evaluate the therapeutic efficacy of different treatments. As shown in Figure 3 d–e, the temperature of arthritic knees was  $\approx 4^\circ\text{C}$  higher than that of healthy knee joints. In comparison, the temperature of knee joints was dramatically lowered for OA rats after treatment with pPADN or Dex-p; Dex-pPADN treatment further decreased

this value to the lowest level seen. These findings suggest that Dex-pPADN has robust efficacy for OA treatment.

To further assess the therapeutic effect of Dex-pPADN, micro-CT imaging was applied to analyze bone morphology and bone microstructure. As shown in Figure 3 f, severe bone and cartilage erosion occurred around inflamed knee joints in the OA model group, but only slight articular cartilage degradation was observed after pPADN or Dex-p treatment. In particular, there were nearly no pathological changes in inflamed knee joints after treatment with Dex-pPADN. The relevant indicators of bone structure were further calculated and compared through histomorphometric analysis of CT images. BV/TV (Bone Volume/Total Volume) is generally

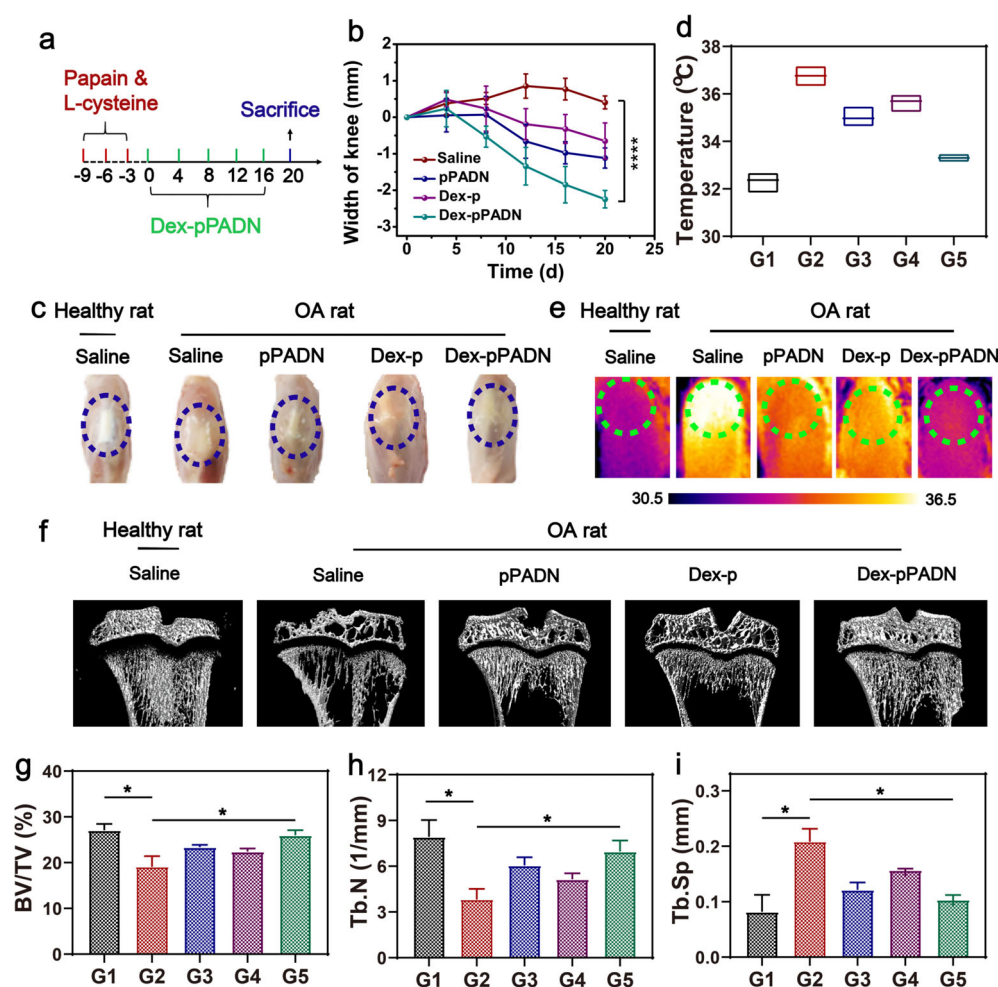


**Figure 3.** Therapeutic efficacy of Dex-pPADN in OA rat model. a) Schematic illustration of the establishment and treatment schedule of the OA model. b) Knee width change of OA rats at various time points after different treatments. c) Representative digital images of knee joints in different groups. d) Quantification of knee joint temperature in different groups. e) Representative thermographic images of healthy knees or arthritic knees with different treatments. f) Representative CT images of healthy knees and arthritic knees with different treatments. g–i) Quantitative analysis of Bone Volume/Total Volume (BV/TV), Trabecular Number (Tb.N), and Trabecular Separation (Tb.Sp) of knee joints in different groups. G1: healthy rats; G2–G5: OA rats (G2: saline treatment; G3: pPADN treatment; G4: Dex-p treatment; G5: Dex-pPADN treatment). Statistical significance was calculated by t-test ( $n=4$ ): \*  $p < 0.05$  and \*\*\*\*  $p < 0.001$ .

used to reflect bone mass. Tb.N (trabecular number) and Tb.Sp (trabecular separation) are main factors referring to the spatial structure of trabecular bone. The lowered Tb.N value and increased Tb.Sp value indicate that bone catabolism was greater than bone anabolism.<sup>[22]</sup> As shown in Figure 3 g–i, the BV/TV value was dramatically lower in the OA model group compared to healthy rats. In addition, significant lower Tb.N and higher Tb.Sp were also observed in OA model group, indicating osteoporosis. In comparison, Dex-pPADN treatment remarkably restored these indicators to near-normal levels. Taken together, these results suggest that Dex-pPADN significantly prevented OA-mediated cartilage erosion and bone destruction.

Furthermore, the therapeutic efficacy of Dex-pPADN was analyzed by histological examination (Figure 4 a–d). H&E stained images of knee joints from the OA model group showed severe bone destruction, neutrophil infiltration, and

massive synovial villous hyperplasia, which are typical symptoms of OA. In comparison, treatment with Dex-pPADN showed almost no synovial hyperplasia or cartilage erosion. Safranin O staining was then performed to assess cartilage degradation and extracellular cartilage matrix (ECM) changes. Articular cartilage in healthy rats clearly exhibited strong expression of proteoglycans. However, in the OA model group, articular cartilage was severely damaged, accompanied by weak distribution of proteoglycans in ECM. After treatment with Dex-pPADN, these symptoms were efficiently alleviated, as evidenced by the almost-intact cartilage surface and evenly distributed proteoglycans in ECM. The therapeutic effect of Dex-pPADN in inhibiting the degradation of cartilage ECM was further confirmed by immunofluorescence staining analysis of aggrecan levels. As shown in Figure 4 a, aggrecan was severely depleted in cartilage ECM of OA rats, but uniformly distributed in the Dex-pPADN treatment group. L-DOPA with catechol structure has been suggested as an effective anti-

oxidant. Therefore, we also used L-DOPA as a ROS scavenging control to study if it has the same ability to reduce symptoms (Figure S33). Results showed that L-DOPA moderately alleviated the cartilage erosion and a small amount of aggrecan was present in ECM.

To evaluate the systemic response of Dex-pPADN, serum levels of TNF- $\alpha$ , IL-12, and IL-1 $\beta$  in rats subjected to various treatments were assessed (Figure 4 e–g). These pro-inflammatory cytokines were significantly upregulated accompanying the establishment of OA. Conversely, these cytokines were decreased in Dex-p, pPADN, and Dex-pPADN treatment groups. In particular, the Dex-pPADN treatment group showed the lowest levels of these pro-inflammatory cytokines. These results suggest that Dex-pPADN not only effectively alleviated synovitis and degradation of cartilage and its extracellular matrix, but also suppressed the over-expression of pro-inflammatory factors.



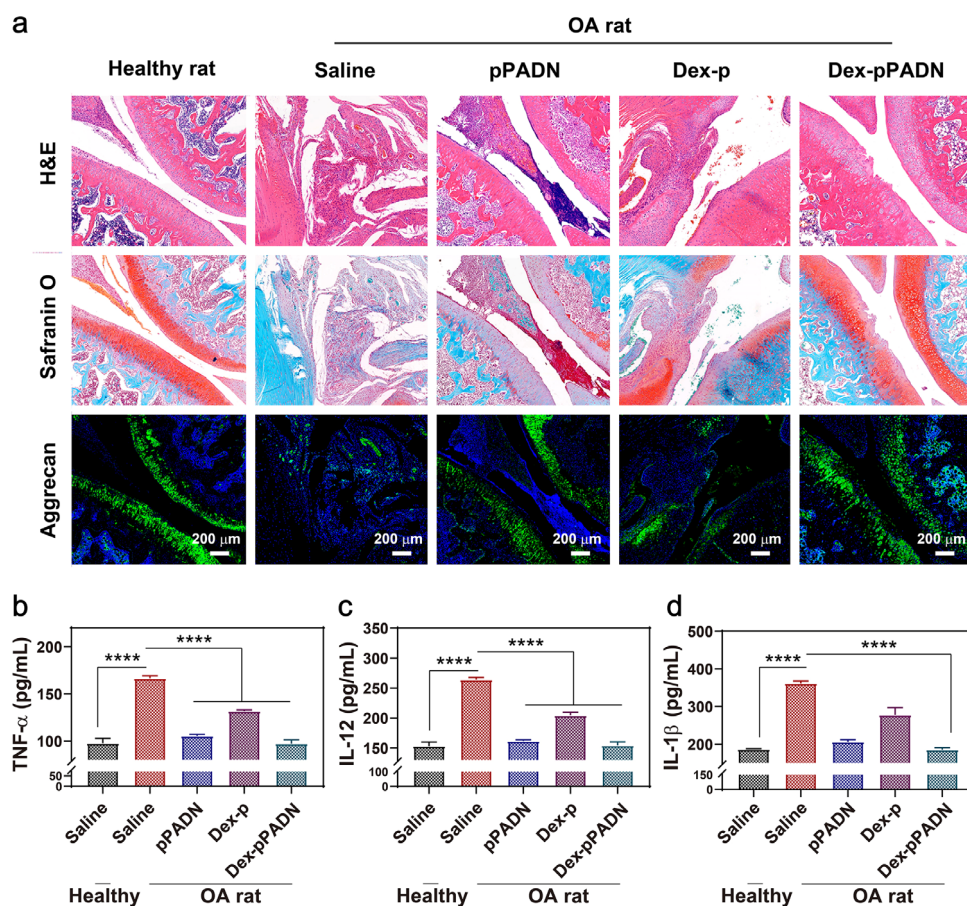


**Figure 4.** Histopathology analysis and inflammation evaluation of OA rats. a) H&E staining images, safranin O staining images, and immunofluorescence staining images of knee joints in different groups. Serum levels of b) TNF- $\alpha$ , c) IL-12, and d) IL-1 $\beta$  in rats with different treatments. Statistical significance was calculated by t-test ( $n=4$ ): \*  $p < 0.05$ , \*\*  $p < 0.01$ , \*\*\*  $p < 0.005$ , and \*\*\*\*  $p < 0.001$ .

To assess the potential side-effects of Dex-pPADN, the main organs in all groups were harvested and subjected to H&E staining at the end of treatment. As shown in Figure S34, no obvious tissue damage was found in Dex-pPADN or pPADN treatment groups, whereas slight hemorrhage and necrosis were detected in liver and kidney in the Dex-p treatment group. Furthermore, Dex-pPADN and Dex-p were intravenously injected into rats every fourth day for 5 times. After 20 days, the major organs were collected for H&E staining (Figure S35). Damaged renal tubules were found in kidney tissues from the Dex-p treated rats, and vacuolar degeneration could be clearly observed in liver sections. In comparison, much fewer damaged structures were noticed in the saline or Dex-pPADN group. These results suggest that the specific encapsulation with pPADN effectively reduced the adverse effects of Dex.

On the basis of the structural transformation of Dex-pPADN under an oxidative microenvironment, we explored the additional ability of Dex-pPADN to monitor OA progression by imaging the inflammation-associated ROS using an in vivo PA imaging system. At the study endpoint, all rats received intra-articular injection of Dex-pPADN; PA imaging in the articular cavity region was carried out. As shown in Figure 5a–d, the knee joints of healthy rats

displayed continuous low PA signals at all investigated time points. However, knee joints in the OA model group showed an initial low PA signal, whose intensity increased with time, reaching a maximum 2 h post injection. In contrast, only a small enhancement in PA signal was observed over time after treatment with pPADN or Dex-p. In the case of Dex-pPADN, the PA signal in knee joint region was still quite low 2 h post injection, close to that in the healthy group. Overall, these results indicate that Dex-pPADN can act as a PA contrast agent to achieve effective diagnosis and treatment guidance for OA.

The feasibility of monitoring OA progression via assessing inflammation-associated ROS was further verified using a conventional ROS-sensitive luminescent probe L-012. At the end of treatment, L-012 was delivered to the knee joint region of all rats via intra-articular injection. Luminescent signals were noninvasively monitored via an in vivo imaging system. As shown in Figure 5e,f, the luminescent signal in inflamed knee joints was stronger than that in healthy knee joints. After treatment with various drug formulations, the decrease in the intensity of luminescent signals in inflamed regions was observed. Consistent with the PA imaging results, the luminescent signal in the Dex-pPADN treatment group was weakest, indicating not only effective mitigation of oxidative stress and inflammatory responses of Dex-pPADN in OA rats, but also the potential to identify inflammatory regions and monitor treatment outcomes.

## Conclusion

In conclusion, we have developed a Dex-pPADN platform and demonstrated its potential as an anti-inflammatory strategy in OA management. Unlike existing anti-inflammatory drug carriers, pPADN (prepared from an amphiphilic phenylboronic acid-decorated L-DOPA derivative) provided a scaffold for reversible coupling with glucocorticoids to facilitate ROS- and pH-responsive self-assemblies of glucocorticoids based on 1,3-diol/phenylboronic acid chemistry and hydrophobic interaction. This is the first demonstration of

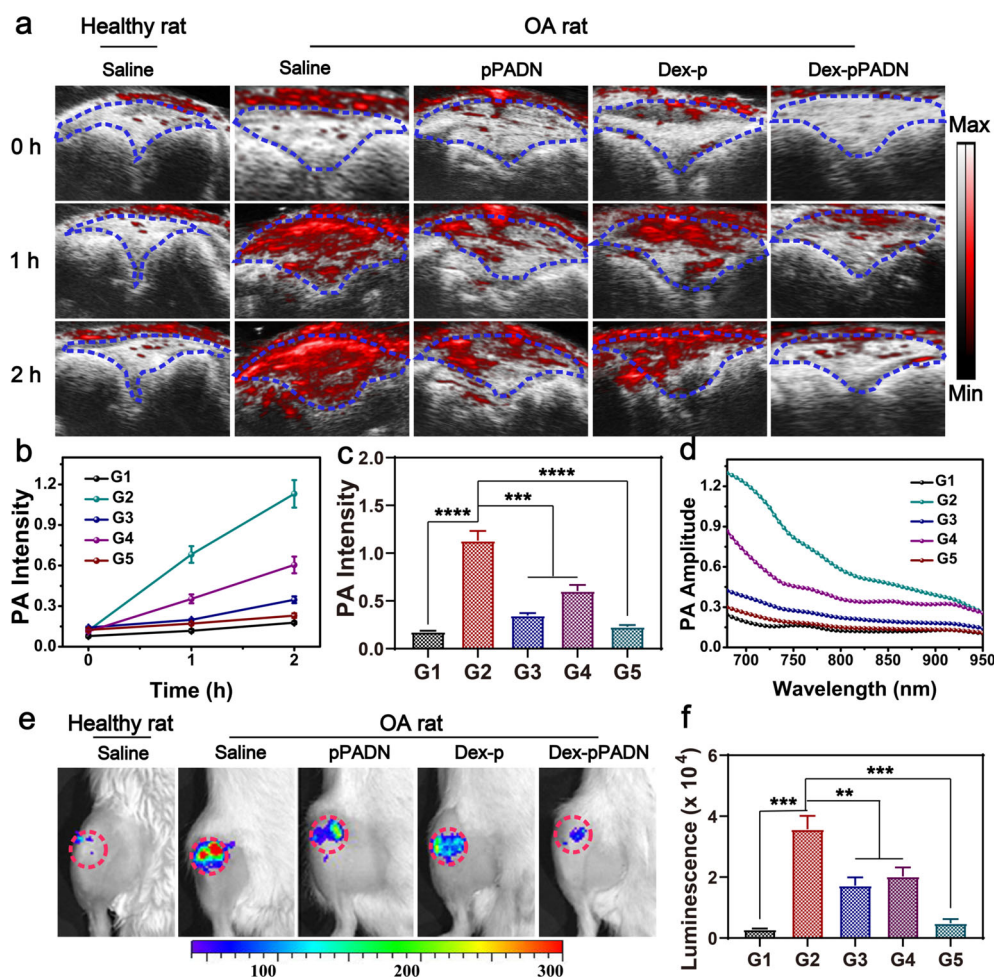


**Figure 5.** In vivo therapeutic monitoring via evaluation of ROS levels in OA rats with different treatments. a) Representative PA images of a healthy articular cavity or an arthritic articular cavity with different treatments. b) PA signal intensity of Dex-pPADN (excited at 710 nm) at various time points in different groups. c) PA signal intensity at 710 nm in different groups after injection with Dex-pPADN for 2 h. d) PA spectra of Dex-pPADN in different groups after injection with Dex-pPADN for 2 h. (b–d: G1: healthy rats; G2: OA rats treated with saline; G3: OA rats treated with pPADN; G4: OA rats treated with Dex-p; G5: OA rats treated with Dex-pPADN). e) In vivo luminescence images of healthy knees and arthritic knees in rats with different treatments. f) Corresponding L-012 luminescence intensity in different groups. (G1: healthy rats; G2: OA rats treated with saline; G3: OA rats treated with pPADN; G4: OA rats treated with Dex-p; G5: OA rats treated with Dex-pPADN). Statistical significance was calculated by t-test ( $n=3$ ): \*  $p < 0.05$ , \*\*  $p < 0.01$ , \*\*\*  $p < 0.005$ , and \*\*\*\*  $p < 0.001$ .

specific delivery and on-demand activation of glucocorticoids in the inflamed microenvironment via phenylboronic acid-based polymeric nanocarriers. Moreover, through the cascade of oxidation and polymerization reactions, pPADN demonstrated ROS-triggered structural transformation to form melanin-like structures at the site of inflammation, displaying superb antioxidative activity. By synergetic anti-oxidation and anti-inflammatory effects, Dex-pPADN demonstrated greater efficacy than either Dex-p or pPADN in OA treatment, effectively suppressing articular cartilage destruction and extracellular matrix degradation. In addition, Dex-pPADN has potential as an effective PA contrast agent for noninvasive tracing and monitoring of OA therapy via structural transformation upon ROS trigger. Taken together, this system holds exciting promise for the development of biomaterials in

addressing inflammation-related diseases and improving glucocorticoid-based treatment of inflammation.

### Acknowledgements

This work was supported by the Prostate Cancer Foundation Young Investigator Award, the National Natural Science Foundation of China (Nos. 21874024; 51973084), and the joint research projects of Health and Education Commission of Fujian Province (2019-WJ-20), and the Natural Science Foundation of Fujian Province (No. 2020J02012).

### Conflict of interest

The authors declare no conflict of interest.

**Keywords:** antioxidants · drug delivery · inflammation · L-DOPA · photoacoustic imaging

- [1] a) M. E. Kotas, R. Medzhitov, *Cell* **2015**, *160*, 816–827; b) K. L. Rock, E. Latz, F. Ontiveros, H. Kono, *Annu. Rev. Immunol.* **2010**, *28*, 321–342; c) A. D. Luster, R. Alon, U. H. von Andrian, *Nat. Immunol.* **2005**, *6*, 1182–1190.
- [2] a) P. K. Kim, C. S. Deutschman, *Surg. Clin.* **2000**, *80*, 885–894; b) J. C. de Grauw, C. H. A. van de Lest, P. R. van Weeren, *Arthritis Res. Ther.* **2009**, *11*, R35; c) J. Eppensteiner, R. P. Davis, A. S. Barbas, J. Kwun, J. Lee, *Front. Immunol.* **2018**, *9*, 190.
- [3] a) P. Rajendran, Y. F. Chen, Y. F. Chen, L. C. Chung, S. Tamilselvi, C. Y. Shen, C. H. Day, R. J. Chen, V. P. Viswanadha, W. W. Kuo, C. Y. Huang, *J. Cell. Physiol.* **2018**, *233*, 6458–6471; b) P. Libby, *Nutr. Rev.* **2007**, *65*, 140–146; c) S. F. Moss, M. J. Blaser, *Nat. Clin. Pract. Oncol.* **2005**, *2*, 90–97.
- [4] a) W. L. Wan, Y. J. Lin, P. C. Shih, Y. R. Bow, Q. Cui, Y. Chang, W. T. Chia, H. W. Sung, *Angew. Chem. Int. Ed.* **2018**, *57*, 9875–9879; *Angew. Chem.* **2018**, *130*, 10023–10027; b) W.-L. Wan, Y.-J. Lin, H.-L. Chen, C.-C. Huang, P.-C. Shih, Y.-R. Bow, W.-T. Chia, H.-W. Sung, *J. Am. Chem. Soc.* **2017**, *139*, 12923–12926; c) Y. Liu, J. Shi, *Nano Today* **2019**, *27*, 146–177.
- [5] a) J. Park, J. S. Min, B. Kim, U. B. Chae, J. W. Yun, M. S. Choi, I. K. Kong, K. T. Chang, D. S. Lee, *Neurosci. Lett.* **2015**, *584*,



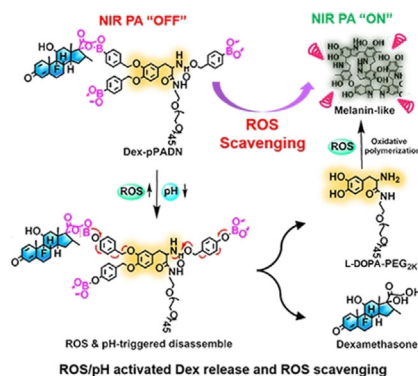
## Research Articles



## Drug Delivery

C. Zhao, J. Chen, J. Ye, Z. Li, L. Su,  
J. Wang, Y. Zhang, J. Chen, H. Yang,  
J. Shi,\* J. Song\*

Structural Transformative Antioxidants  
for Dual-Responsive Anti-Inflammatory  
Delivery and Photoacoustic Inflammation  
Imaging



PEGylated, phenylboronic acid modified L-DOPA-derived nanoparticles (pPADN) specifically integrated reactive oxygen species (ROS) scavenging and anti-inflammatory drug delivery to treat osteoarthritis. The pPADN sensed and eliminated elevated ROS via cascade oxidative reactions and delivered glucocorticoids to the site of inflammation.